Spectroscopic and Calorimetric Characterizations of DNA Duplexes Containing 2-Aminopurine†

Scott M. Law,‡ Ramon Eritja,§ Myron F. Goodman,|| and Kenneth J. Breslauer*,‡

Department of Chemistry, Rutgers—The State University of New Jersey, Piscataway, New Jersey, 08855, European Molecular Biological Laboratories, Heidelberg, Germany 69117, and Department of Biological Sciences, Hedco Molecular Biology Laboratories, University of Southern California, Los Angeles, California 90089-1340

Received June 18, 1996; Revised Manuscript Received August 2, 1996⊗

ABSTRACT: The base analog 2-aminopurine (AP) strongly promotes A·T to G·C and G·C to A·T transitions in bacteria and bacteriophage. During DNA replication, the primary mutagenic event involves formation of a heteroduplex with an AP·C site at a much higher frequency than formation of the corresponding heteroduplex with an A·C site. It is not known if AP-induced mutagenesis correlates with differences in the thermodynamic properties of an AP·C versus an A·C site, or whether interactions involving DNA polymerases are controlling. To address this specific question, and more generally to characterize AP-containing duplexes, we have used a combination of spectroscopic and calorimetric techniques to determine the thermodynamic properties of six 11-mer duplexes. The sequences of these duplexes are identical except for the identity of the variable central base pair which can be either A·T, A·C, AP·T, AP·C, AP·A, or AP·G, and which we use to designate each duplex. Analyses and interpretation of the optically and calorimetrically derived thermal and thermodynamic data on these six duplexes reveal the relative stabilizing influence of the central base pairs to be A·T > AP·T > AP·C > AP·A > AP·G > A·C, with the AP·C-containing duplex being significantly more stable than the A·C-containing duplex. In the aggregate, our results suggest that during incorporation, base pair discrimination by DNA polymerases is influenced, in part, by differences in the thermodynamic stabilities of the newly formed base pairs.

The base analog 2-aminopurine (AP)[1] *in vivo* induces A·T → G·C and G·C → A·T transitions in bacteria and bacteriophages (Freese, 1959). When added to growing bacteria, AP is metabolized to form deoxy-2-aminopurine triphosphate (dAPTP) (Rogan & Bessman, 1970) which serves as a substrate for DNA polymerases (Bessman et al., 1974; Muzyczka et al., 1972). The proposed pathway for the A·T → G·C transition mutation involves incorporation of deoxy-2-aminopurine monophosphate (dAPMP) to form an AP·T base pair during replication, followed by incorporation of dCMP opposite AP in a subsequent round of replication (Freese, 1959). Figure 1 schematically represents this cascade of events. In the G·C → A·T pathway, dAPMP is incorporated opposite a template C residue, followed by incorporation of dTMP opposite the AP residue. During replication, AP·T and AP·C sites are formed at higher frequencies than mismatched base pairs which involve the naturally occurring nucleotides. Consequently, AP has been used extensively to study DNA polymerase fidelity [see Goodman et al. (1993) and references cited therein].

According to one proposed model (Galas & Branscomb, 1978), the ratio of the insertion frequencies of a mismatched base to the proper base is dictated by their difference in free energies ($\Delta\Delta G°$) (Clayton et al., 1979; Watanabe & Goodman, 1982; Mhaskar & Goodman, 1984). Using experimentally determined insertion frequencies, this model predicts $\Delta\Delta G°$ values of ≈1.1 kcal mol^{-1} between an A·T and an AP·T bp (Galas & Branscomb, 1978; Clayton et al., 1979), and ≈1.8 kcal mol^{-1} between an AP·T and an AP·C bp (Watanabe & Goodman, 1982). The corresponding $\Delta\Delta G°$ values experimentally determined in this work are qualitatively consistent with these predicted values, thereby lending credance to the proposed model which argues for a

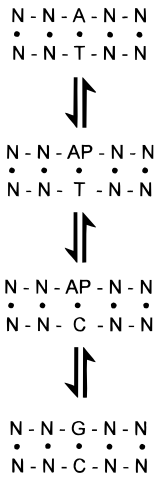

FIGURE 1: Proposed pathway for DNA polymerase-mediated A·T ↔ G·C transitions caused by incorporation of AP. Each drawing represents a portion of the DNA duplex after a successive round of replication.

† This work was supported by National Institutes of Health Grants GM21422 and AG11398 (M.F.G.), North Atlantic Treaty Organization Collaborative Research Grant 900554 (M.F.G.), and National Institutes of Health Grants GM23509 and GM34469 (K.J.B.).

* To whom correspondence should be addressed. Telephone: 908-445-3956. Fax: 908-445-3409.

‡ Rutgers—The State University of New Jersey.

§ European Molecular Biology, Laboratories.

|| University of Southern California.

⊗ Abstract published in *Advance ACS Abstracts,* September 15, 1996.

[1] Abbreviations: AP, 2-aminopurine; NMR, nuclear magnetic resonance spectroscopy; bp, base pair(s).

S0006-2960(96)01454-7 CCC: $12.00

thermodynamic basis for incorporation discrimination during replication.

Owing to its fluorescence properties, the AP base analog recently has been used as a real-time reporter molecule to study the dynamics of DNA duplexes (Guest et al., 1991), as well as the fidelity of DNA synthesis (Bloom et al., 1993, 1994). To date, T_m (Eritja et al., 1986), time-resolved fluorescence (Guest et al., 1991), NMR (Fagan et al., 1996; Fazakerley et al., 1987; Sowers et al., 1986b), and pre-steady-state kinetic (Bloom et al., 1993, 1994; Frey et al., 1995) studies have been conducted on AP-containing duplexes. However, still lacking are thermodynamic characterizations of such duplexes. Consequently, it has not yet been possible to determine to what extent discrimination of nucleotide insertion during replication occurs at the thermodynamic level. To address this question, and more generally to characterize AP-containing structures thermodynamically, we have synthesized six 11-mer sequences which can be hybidized to form duplexes that are identical except for the central base pair, which is either A·T, AP·T, AP·C, AP·A, AP·G, or A·C. We have used differential scanning calorimetry and a van't Hoff analysis of optical melting data to characterize the thermodynamic properties of each duplex. The resulting data yield $\Delta\Delta G°$ values which are consistent with the biologically observed enhanced formation of AP·T versus A·T sites, and AP·C versus AP·T sites.

MATERIALS AND METHODS

Oligonucleotides. Oligonucleotide Synthesis and Purification. We used an Applied Biosystems DNA synthesizer, Model 392, in conjunction with commerically available nucleoside phosphoramidites and solid supports to produce two families of 11-mers with the sequences 5′GCATGXGTACG3′ and 5′CGTACYCATGC3′, where X = A, C, T, and G, and Y = AP and A. The AP phosphoramidite was prepared as previously described (Connolly, 1991). Purification of the oligonucleotides was performed using reverse-phase HPLC and standard "DMT on" and "DMT off" protocols. Details are provided in Connolly (1991). After purification, the oligonucleotides were converted to their sodium salts. Overall yields were about 40 OD units/μmol synthesis (40% yield). Homogeneity of the resulting purified oligonucleotides was checked by gel electrophoresis.

Molar extinction coefficients (ϵ) for the single-stranded oligonucleotides were determined by phosphate analysis (Snell & Snell, 1949) and are listed in Table 1A, along with the abbreviations used in this work to designate each strand. The stoichiometries of the six complexes formed by pairwise mixing of the strands were determined using previously described methods (Plum et al., 1995). The resulting "mixing curves" (not shown) indicate that all complexes exhibit a 1:1 stoichiometry, consistent with duplex formation. The total hyperchromicity changes observed for duplex formation relative to the single strand ranged from 14% to 19%.

Optical Spectra and Melting Curves. All optical measurements (UV, CD, and fluorescence) were performed in a buffer consisting of 10.0 mM PO_4, 1.0 mM EDTA, pH 7.00, with the [Na^+] varying from 0.030 to 1.00 M. The UV absorbance measurements were performed on a Perkin Elmer Lambda 4C spectrophotometer or an AVIV 14 DS spectrophotometer. The CD measurements were made using an AVIV C60 spectropolarimeter at a total strand concentration (C_T) of 16 μM, and a [Na^+] of 1.00 M. The fluorescence measurements were made using a Perkin Elmer MPF 66 spectrofluorometer in a buffer consisting of 10.0 mM PO_4, 1.0 mM EDTA, and 1.00 M Na^+, pH 7.0, at a C_T of 16 μM, unless otherwise noted. UV, CD, and fluorescence melting experiments were performed by ramping the temperature in 0.5 °C steps or in linear fashion at rates of 0.1 or 0.5 °C min^{-1}.

Differential Scanning Calorimetry (DSC). Calorimetric measurements were performed using a Microcal MC-2 differential scanning instrument at a scan rate of 1.0 °C min^{-1} in a buffer consisting of 50.0 mM PO_4, 1.0 mM EDTA, and 1.00 M Na^+, pH 7.0. Data were analyzed using previously described protocols (Breslauer, 1995; Marky & Breslauer, 1987) to obtain model-independent values for $\Delta G°_{cal}$, $\Delta H°_{cal}$, and $\Delta S°_{cal}$.

Extracting Thermodynamic Parameters from Optical Melting Measurements. As previously described (Breslauer, 1995; Marky & Breslauer, 1987), one can derive the van't Hoff enthalpy change for a duplex to single-strand transition from a single optical melting profile by two methods. In both methods, the experimental absorbance versus temperature (T) curve initially is converted into an α versus T profile, where α represents the fraction of the duplex in the single-stranded state. In one approach, the slope of the transition at the melting temperature, T_m (where $\alpha = 0.5$), is measured $[(\partial\alpha/\partial T)_{T_m}]$ and the van't Hoff transition enthalpy, $\Delta H°_{vH}$, is calculated using the expression:

$$\Delta H°_{vH} = 6RT_m^2\left(\frac{\partial\alpha}{\partial T}\right)_{T_m} \quad (1)$$

In a second approach, one calculates the derivative curve, $\partial\alpha/\partial(1/T)$, from the α versus T melting profile and determines $\Delta H°_{vH}$ from the transition breadth using the expression:

$$\Delta H°_{vH} = \frac{10.14}{(1/T_1) - (1/T_2)} \quad (2)$$

where T_1 and T_2 are the temperatures at the "half height", which corresponds to $\partial\alpha/\partial(1/T)$ at a value which is 50% of the maximum $\partial\alpha/\partial(1/T)$ value. In both analyses, ΔC_p is assumed to be zero.

In addition to the two analyses of single melting profiles noted above, thermodynamic data also can be obtained by analyzing the concentration dependence of the T_m for a family of melting profiles, as previously described (Marky & Breslauer, 1987; Breslauer, 1995; Aboul-ela et al., 1985). Specifically, for a duplex formed from two complementary strands, a plot of $1/T_m$ vs ln C_T should yield a straight line which can be represented by the two-state equation:

$$\frac{1}{T_m} = \frac{R}{\Delta H°}\ln C_T + \frac{\Delta S° - R\ln 4}{\Delta H°} \quad (3)$$

From such a line, $\Delta H°_{vH}$ and $\Delta S°_{vH}$ can be determined from the slope and the y-intercept, respectively, while $\Delta G°_{vH}$ can be calculated at any temperature, assuming a zero heat capacity, using the standard thermodynamic equation $\Delta G° = \Delta H° - T\Delta S°$ (Breslauer, 1995; Marky & Breslauer, 1987).

The difference between the $\Delta G°$ values for two duplexes ($\Delta\Delta G°$) that differ by a specific site alteration frequently is used to define the stabilizing or destabilizing influence of the site modification. Although conceptually reasonable, on

Table 1

(A) Sequence and Extinction Coefficients of Oligonucleotides

sequence	abbreviated strand name	$\epsilon_{260,90°C}$ (M^{-1} cm^{-1})
5′-CGTAC**A**CATGC-3′	A_1	102400
5′-CGTAC**(AP)**CATGC-3′	AP_1	82000
5′-GCATG**T**GTACG-3′	T_2	98130
5′-GCATG**C**GTACG-3′	C_2	119500
5′-GCATG**A**GTACG-3′	A_2	98100
5′-GCATG**G**GTACG-3′	G_2	98600

(B) Duplexes and Designations

duplex sequence	duplex abbreviation
d(CGTAC$\underline{A}$CATGC)·d(GCATG$\underline{T}$GTACG)	A_1·T_2
d(CGTAC$\underline{A}$CATGC)·d(GCATG$\underline{C}$GTACG)	A_1·C_2
d(CGTAC$\underline{AP}$CATGC)·d(GCAT$\underline{G}$TGTACG)	AP_1·T_2
d(CGTAC$\underline{AP}$CATGC)·d(GCATG$\underline{C}$GTACG)	AP_1·C_2
d(CGTAC$\underline{AP}$CATGC)·d(GCATG$\underline{A}$GTACG)	AP_1·A_2
d(CGTAC$\underline{AP}$CATGC)·d(GCATG$\underline{G}$GTACG)	AP_1·G_2

a practical level this approach frequently is compromised by the need to define small differences between large numbers, a problem which is exacerbated by computational coupling between the $\Delta H°$ and $\Delta S°$ data used to calculate $\Delta G°$, and by error propagation which produces $\Delta G°$ data with significant uncertainties. Plum et al. (1995) recently have described a method which combines both optical and calorimetric data in a manner that minimizes these problems. Another alternative approach that also minimizes the problems noted above makes use of a method of data analysis originally described by Gralla and Crothers (1973). Specifically, for two duplexes, A and B, with similar sequences, the difference in the free energies of duplex formation ($\Delta\Delta G°$) can be determined from the differences between the concentrations of oligonucleotides that give the same melting temperature. In our analysis, we chose a T_m value of 30 °C for comparison. The relevant equation is

$$\Delta\Delta G°_{A\rightarrow B} \equiv \Delta G°_B - \Delta G°_A = RT_m[\ln (C_{T,B}) - \ln (C_{T,A})] \quad (4)$$

where $\Delta G°_A$ and $\Delta G°_B$ are the free energy changes for the formation of two different duplexes, and $C_{T,A}$ and $C_{T,B}$ are the total strand concentrations of duplexes A and B that yield identical T_m values, in our case 30 °C. We have used this approach to define the incremental thermodynamic impact of altering the central base pair in the family of duplexes studied here.

Values of Δi, which reflect the number of Na^+ ions per phosphate released upon duplex denaturation, were calculated using the relationship (Olmsted et al., 1991; Record et al., 1978):

$$\Delta i = \frac{\partial(1/T_m)}{\partial \ln [Na^+]} \frac{\Delta H°}{R} \quad (5)$$

RESULTS

UV Equilibrium Melting Curves. We have combined the single-stranded oligonucleotides shown in Table 1A to produce the six duplexes listed in Table 1B, which we designate by the identity of their central base pair: A_1·T_2, A_1·C_2, AP_1·T_2, AP_1·C_2, AP_1·A_2, and AP_1·G_2. We then measured UV melting profiles and used previously described protocols (Breslauer, 1995; Marky & Breslauer, 1987), to determine T_m's for each duplex at various C_T values. The resulting $1/T_m$ vs ln C_T plots are shown in Figure 2, with the lower lines corresponding to the thermally more stable duplexes. Note that we observe the following T_m hierarchy, in order of decreasing thermal stability: A_1·T_2 ≥ AP_1·T_2 > AP_1·C_2 > AP_1·A_2> AP_1·G_2 > A_1·C_2. This T_m hierarchy holds at all strand concentrations since the lines do not cross. A direct comparison of the T_m values at $C_T = 16$ μM is presented in column 2 of Table 2, with the corresponding ΔT_m values, relative to the A·T duplex, being listed in column 3.

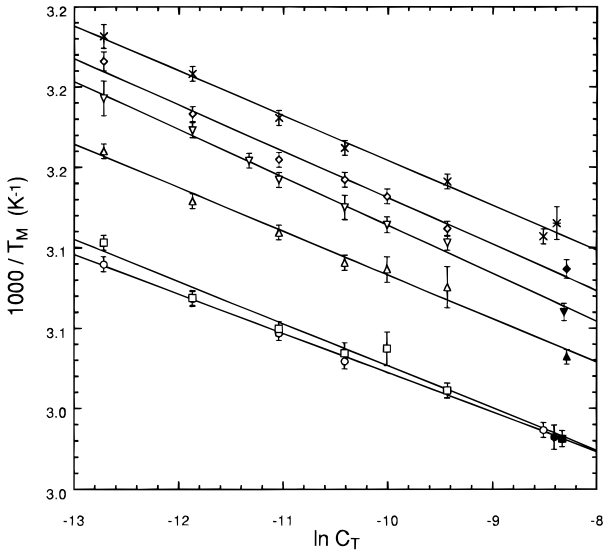

FIGURE 2: Plots of $1/T_m$ vs ln C_T for the six duplexes investigated in this study. (Open circles) A_1·T_2; (open squares) AP_1·T_2; (open triangles) AP_1·C_2; (open inverted triangles) AP_1·A_2; (open diamonds) AP_1·G_2; (X) A_1·C_2. Open symbols [(X) for A_1·C_2] represent values determined from UV melting curves, and filled symbols [(∗) for A_1·C_2] represent values determined from calorimetry. The lines are linear least square fits of the data.

Table 2: Comparison of T_m and van't Hoff Free Energy Data

duplex	T_m (°C)[a]	ΔT_m (°C)	$\Delta\Delta G_{30°C}$ (kcal mol^{-1})[b]
A_1·T_2	55.1 ± 0.4		
AP_1·T_2	54.4 ± 0.4	−0.3 ± 0.6	0.5 ± 0.9
AP_1·C_2	48.5 ± 0.4	−6.6 ± 0.6	1.7 ± 0.8
AP_1·A_2	45.1 ± 0.5	−10.0 ± 0.6	3.1 ± 0.5
AP_1·G_2	43.5 ± 0.3	−11.6 ± 0.5	3.2 ± 0.5
A_1·C_2	41.3 ± 0.4	−13.8 ± 0.6	3.7 ± 0.5

[a] Conditions are 10.0 mM PO_4, and 1.00 mM EDTA, 1.00 M Na^+, pH 7.0; $C_T = 16$ μM. [b] Values are calculated from the data of $1/T_m$ vs ln C_T curves using the method of Gralla and Crothers (1973).

A van't Hoff analysis of the individual UV melting curves ($\Delta H°_{vH}$) permitted us to calculate values for the enthalpy of duplex dissociation. The resulting $\Delta H°_{vH}$ data for all six duplexes are listed in column 2 of Table 3. Note that the $\Delta H°_{vH}$ value of ∼52 kcal mol^{-1} that we calculate for the A_1·C_2 duplex is significantly less than that of the other five duplexes, which exhibit values which range from 68 to 81 kcal mol^{-1}, with the $\Delta H°_{vH}$ hierarchy, in order of decreasing duplex dissociation enthalpy, being A_1·T_2 > AP_1·T_2 ≥ AP_1·C_2 > AP_1·G_2 ≥ AP_1·A_2 > A_1·C_2. With the exception of the relative placement of the AP_1·A_2 and AP_1·G_2 duplexes, this $\Delta H°_{vH}$ hierarchy matches the T_m hierarchy listed in Table 2. While the assumption that $\Delta C_p = 0$ is implicit in this analysis, our DSC measurements reveal this to be a valid assumption.

Table 3: Comparison of van't Hoff Enthalpies, Entropies, and Free Energy Changes Derived from UV Absorbance Melting Data

duplex	ΔH_{vH}[a] (cal mol^{-1})	ΔH_{vH}[b] (cal mol^{-1})	ΔS_{vH}[b] (cal K^{-1} mol^{-1})	$\Delta G_{vH,30°C}$[b] (kcal mol^{-1})
$A_1 \cdot T_2$	78223 ± 4391	81092 ± 1706	222 ± 5	13.8 ± 2.3
$AP_1 \cdot T_2$	75451 ± 5512	75825 ± 4381	207 ± 12	13.1 ± 5.7
$AP_1 \cdot C_2$	74419 ± 4696	74103 ± 4005	206 ± 11	11.7 ± 5.2
$AP_1 \cdot A_2$	69721 ± 4830	66698 ± 2330	185 ± 7	10.6 ± 3.2
$AP_1 \cdot G_2$	71881 ± 3771	69962 ± 2391	196 ± 8	10.5 ± 3.4
$A_1 \cdot C_2$	52624 ± 3644	71129 ± 2558	202 ± 7	9.9 ± 3.3

[a] Determined from analysis of individual UV melting curves. [b] Determined from plots of $1/T_m$ vs ln C_T.

In columns 3 and 4 of Table 3, we list the $\Delta H°_{vH}$ and $\Delta S°_{vH}$ values determined from the slope and intercepts of the plots shown in Figure 2, along with the corresponding $\Delta G°_{vH}$ values calculated at 30 °C using the standard thermodynamic relationship $\Delta G° = \Delta H° - T\Delta S°$. Note that with the exception of the $A_1 \cdot C_2$ duplex, the $\Delta H°_{vH}$ values calculated by this method are similar to those determined from the individual melting curves. More significantly, the $\Delta G°_{vH}$ heirarchy, in order of decreasing stability at 30 °C, is $A_1 \cdot T_2 > AP_1 \cdot T_2 > AP_1 \cdot C_2 > AP_1 \cdot A_2 \approx AP_1 \cdot G_2 > A_1 \cdot C_2$, which matches the T_m hierarchy listed in Table 2. As previously discussed, however (Krug et al., 1976), $\Delta G°_{vH}$ values determined in this manner may suffer from propagated errors in $\Delta H°_{vH}$ and $\Delta S°_{vH}$, as well as from coupling between these two parameters. These features reduce the reliability of such $\Delta\Delta G°_{vH}$ values. This limitation is of concern since the $\Delta\Delta G°$ data are of particular interest in that they define the free energy difference between two duplexes and, therefore, reflect the net thermodynamic impact of the altered central "base pair" site.

To address this limitation, we have used an additional computational approach to determine $\Delta\Delta G°$ values between pairs of duplexes. This approach, which uses eq 4, reduces the potential shortcomings noted above. The $\Delta\Delta G°$ values (at 30 °C) between the $AP_1 \cdot T_2$ duplex and the five other duplexes that result from application of eq 4 are listed in the final column of Table 2. Significantly, for the one pair of duplexes for which a literature comparison exists, the $\Delta\Delta G°$ value we calculate between the $A_1 \cdot T_2$ and $A_1 \cdot C_2$ duplexes (3.7 ± 0.5 kcal mol^{-1}) falls within the range of previously reported mismatch values (3.9−5.2 kcal mol^{-1}) (Aboul-ela et al., 1985). More generally, our data reveal that the thermodynamic impacts ($\Delta\Delta G°$) of the lesion sites depend on both the presence and the absence of the modified base and the identity of its cross-strand partner, features that will be elaborated on in the Discussion.

Fluorescence Spectroscopy and Equilibrium Melting Curves. Unlike the naturally occurring bases, 2-aminopurine is fluorescent when free in solution or when present in an oligonucleotide. For the AP_1 11-mer shown in Table 1A, the steady-state fluorescence excitation and emission spectra (Figure 3) exhibit a Stokes shift of 61 nm, with maxima at 308 and 369 nm, respectively. Both of these spectra are similar to those previously reported for other oligonucleotide sequences containing the AP base (Guest et al., 1991).

We also have assessed the impact of duplex formation on AP fluorescence. Figure 4 shows the fluorescence emission spectra of a sample containing the AP_1 and T_2 strands at 10 and 90 °C, temperatures at which the strands exist in the duplex and single-stranded states, respectively. Inspection

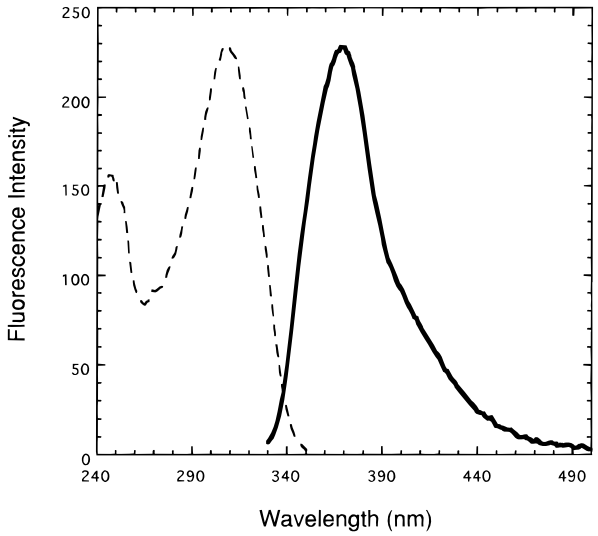

FIGURE 3: Fluorescence emission (solid line) and excitation (dashed line) spectra of an 8 μM solution of the AP_1 strand (in 10.0 mM PO_4, 1.0 mM EDTA, and 1.00 M Na^+, pH 7.0). For the excitation spectra, the emission was monitored at 369 nm, while for the emission spectra, the excitation wavelength was 309 nm. Both spectra were determined using a 5 nm band-pass.

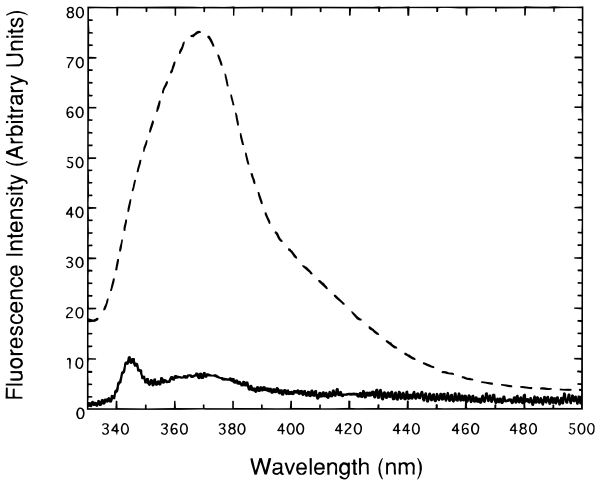

FIGURE 4: Emission spectra of the duplex $AP_1 \cdot T_2$ at 10 °C (solid line) and 90 °C (dashed line). Total strand concentration was 16 μM (8 μM duplex), and the excitation wavelength was 309 nm.

of these spectra reveals that between these two temperatures, we observe an 11-fold difference in fluorescence at 369 nm. This feature, which also is observed with the other cross-strand residues, makes it possible to determine fluorescence equilibrium melting curves, as shown in Figure 5 for the four $AP_1 \cdot X_2$ duplexes, where X = A, C, G, and T.

Inspection of these fluorescence melting profiles reveals a difference in behavior between the lower and upper base lines. By comparison with the absorbance melting profiles, the lower base line is unremarkable, while the upper base line is notable in that it slopes downward. This behavior reflects the temperature dependence of AP fluorescence within the single strand, which probably is due to enhanced quenching that results from increased collisions between the AP base and the solvent in the single-stranded state at elevated temperatures, rather than single-strand aggregation, since the upper base lines in the CD and UV melting profiles are unremarkable. To appropriately correct for this final base line, we independently determined the temperature dependence of the fluorescence for the AP-containing single strand.

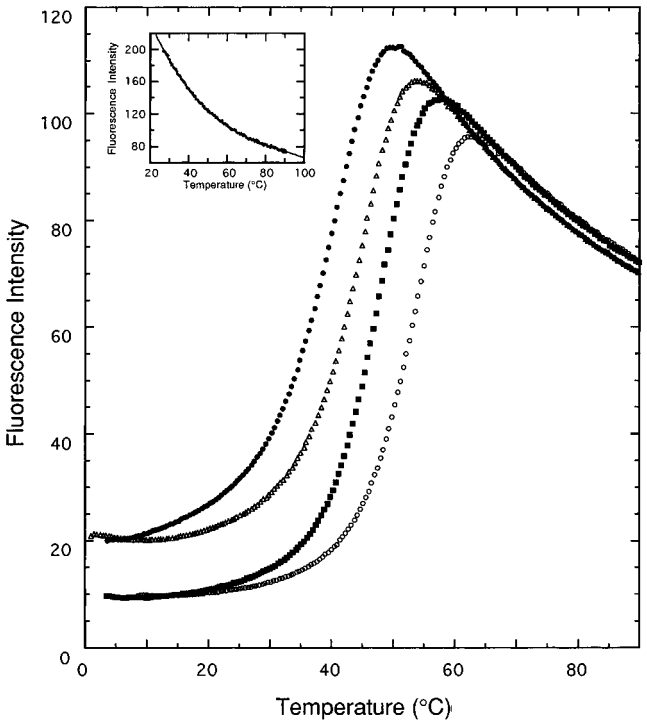

FIGURE 5: Raw data from fluorescence-monitored equilibrium melting curves. (Open circles) $AP_1{\cdot}T_2$; (filled squares) $AP_1{\cdot}C_2$; (open triangles) $AP_1{\cdot}A_2$; (filled circles) $AP_1{\cdot}G_2$. Inset: Fluorescence intensity of the AP_1 strand as a function of temperature. Open symbols represent data points, and the line is the result of a third-order polynomial fit to the data.

Table 4: T_m and van't Hoff Enthalpies Derived from Fluorescence-Monitored Melting Curves

duplex	T_m (°C)	$T_{m,UV} - T_{m,Fluor}$ (°C)	ΔH_{vH} (cal mol^{-1})
$AP_1{\cdot}T_2$	52.8 ± 0.3	1.6 ± 0.5	84753 ± 1600
$AP_1{\cdot}C_2$	48.0 ± 0.3	0.5 ± 0.5	79632 ± 1492
$AP_1{\cdot}A_2$	44.4 ± 0.3	0.7 ± 0.6	77186 ± 2811
$AP_1{\cdot}G_2$	41.3 ± 0.3	2.5 ± 0.4	71506 ± 2318

The resulting profile, which is shown in the inset to Figure 5, can be described by a third-order polynomial, which we used in our analysis of the fluorescence melting profiles by applying protocols analogous to those employed for evaluating the corresponding UV absorbance melting curves.

The resulting T_m and $\Delta H°_{vH}$ data are listed in Table 4, along with a comparison of the absorbance and fluorescence-derived T_m values. Inspection of the fluorescence-based data reveals the T_m and $\Delta H_{°vH}$ hierarchies to be coincident, and equal to $AP_1{\cdot}T_2 > AP_1{\cdot}C_2 > AP_1{\cdot}A_2 > AP_1{\cdot}G_2$. Further note that the fluorescence-based T_m hierarchy matches that derived from the absorbance melting curves. Figure 6 presents a direct comparison of the absorbance and fluorescence melting curves, with the corresponding differential T_m values being listed in the third column of Table 4. We elaborate in the Discussion on the significance of these T_m differences.

CD Spectroscopy. Panel A of Figure 7 shows the CD spectra of the $A_1{\cdot}T_2$ Watson−Crick duplex and the $A_1{\cdot}C_2$ mismatch duplex at 20 °C. Note that both spectra are qualitatively similar. Each spectrum exhibits large positive bands at 224 and 280 nm, and a large negative band at 253 nm, with the intensity of the negative band being equal to or larger than the intensity of the positive band at 280 nm. In short, the CD spectra suggest globally similar duplex

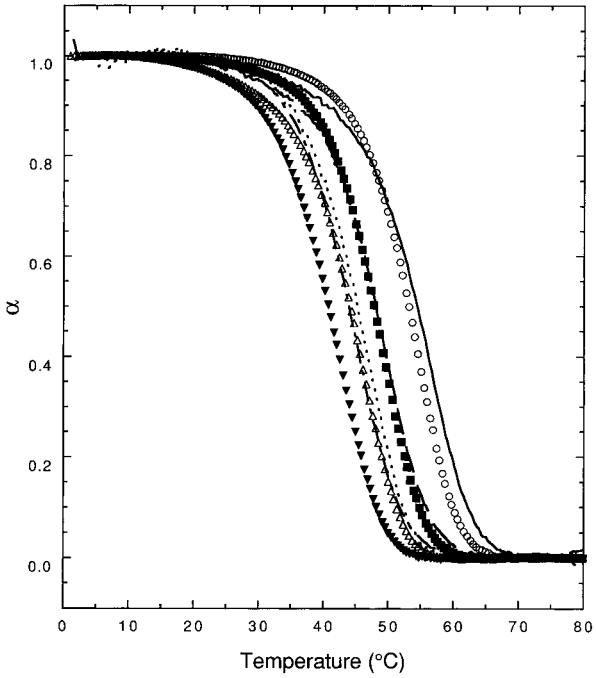

FIGURE 6: Plots of α (fraction of strands in the duplex state) as a function of temperature monitored by either UV absorbance or fluorescence detection. Data from fluorescence experiments are shown as symbols, and data from UV experiments are shown as lines. (Open circles, solid line) $AP_1{\cdot}T_2$; (filled squares, dashed line) $AP_1{\cdot}C_2$; (open triangles, dotted line) $AP_1{\cdot}A_2$; (filled inverted triangles, dashed−dotted line) $AP_1{\cdot}G_2$. Conditions for each experiment are: $C_T = 16\ \mu M$; 10.0 mM PO_4, 1.0 mM EDTA, and 1.00 M Na^+, pH 7.0.

conformations despite the significant thermodynamic differences we have measured (Tables 2 and 3). In other words, isoconformational does not necessarily imply isoenergetic, a feature we previously have noted in our studies of duplexes with other lesions (Plum et al., 1995).

Panel B of Figure 7 shows the CD spectra for the family of $AP_1{\cdot}X_2$ duplexes, where X = T, C, A, or G. Note that all the spectra exhibit positive bands at 223 and 280 nm, and a large negative band at 255 nm. More quantitatively, all four $AP_1{\cdot}X_2$ duplexes have similar molar ellipticities (θ) at 223 and 280 nm, with one exception: at 280 nm, θ for the $AP_1{\cdot}C_2$ duplex is significantly larger than that for the other three $AP_2{\cdot}X_2$ duplexes. Also note that, for each duplex, the magnitude of θ at 255 nm is equal to or larger than the magnitude of θ at 280 nm, although the magnitude of θ at 255 nm differs among the four $AP_1{\cdot}X_2$ duplexes, ranging from -1.3×10^5 deg M^{-1} cm^{-1} for $AP_1{\cdot}G_2$ to -3.2×10^5 deg M^{-1} cm^{-1} for $AP_1{\cdot}C_2$.

One can compare the CD spectra of the $A_1{\cdot}T_2$ and $AP_1{\cdot}T_2$ duplexes in panel C of Figure 7 to assess the conformational impact of the "nascent" lesion on a natural Watson−Crick site. Although both spectra are qualitatively similar, there are two quantitative differences. First, for the $A_1{\cdot}T_2$ duplex, the large negative band is centered around 253 nm, while for the $AP_1{\cdot}T_2$ duplex it is centered at 255 nm. Second, the magitude of θ at 223 nm is significantly larger for the $AP_1{\cdot}T_2$ duplex (1.5×10^5 deg M^{-1} cm^{-1}) than for the $A_1{\cdot}T_2$ duplex (0.8×10^5 deg M^{-1} cm^{-1}). Unfortunately, CD theory is not sufficiently developed to interpret small spectral differences in terms of specific structural/electronic alterations. Consequently, we cannot be more specific about the micro-

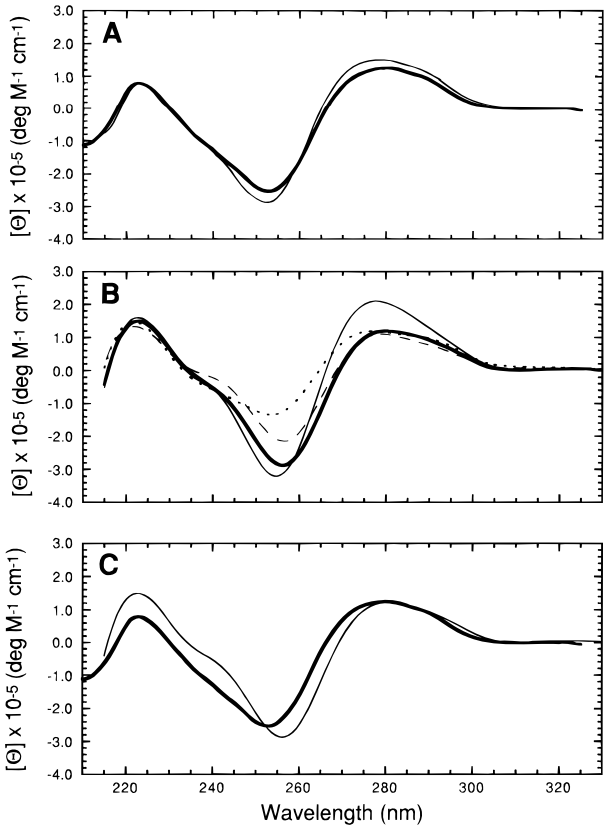

FIGURE 7: CD spectra for all six duplexes investigated. (A) (Thick line) $A_1{\cdot}T_2$ and (thin line) $A_1{\cdot}C_2$. (B) (Thick line) $AP_1{\cdot}T_2$, (thin line) $AP_1{\cdot}C_2$, (dashed line) $AP_1{\cdot}A_2$, and (dotted line) $AP_1{\cdot}G_2$. (C) (Thick line) $A_1{\cdot}T_2$ and (thin line) $AP_1{\cdot}T_2$. Experimental conditions are $C_T = 16\ \mu$M; 10.0 mM PO_4, 1.0 mM EDTA, and 1.00 M Na^+, pH 7.0, at 20 °C.

scopic origins of the differences we observe in the CD spectra.

Salt Dependence. For each duplex, we determined T_m values over a range of $[Na^+]$ between 0.030 and 0.225 M. Figure 8 shows the resulting T_m vs ln $[Na^+]$ plots, while Table 5 lists the corresponding $\partial T_m/\partial$ ln $[Na^+]$ slopes along with the Δi values calculated using eq 5.

Differential Scanning Calorimetry (DSC). Figure 9 shows the calorimetrically measured excess heat capacity (C_p) versus temperature profiles for all six duplexes. The duplex dissociation enthalpies, $\Delta H°_{cal}$, and entropies, $\Delta S°_{cal}$, derived from analyses of these curves are listed in Table 6, along with the corresponding $\Delta G°_{cal}$ values calculated at 30 °C. Comparison of these model-independent calorimetric data with the corresponding model-dependent van't Hoff values listed in Table 3 reveals two features worthy of note. First, we find qualitative, but not quantitative, agreement between the enthalpy and entropy data derived calorimetrically and optically. Given the substantial assumptions involved in the van't Hoff analysis, only qualitative agreement is to be expected, particularly when the data are derived from changes in different observables (heat capacity versus absorbance). Consequently, it would be inappropriate to use these data to assess if the transitions occur in a two-state manner. Second, note that the absolute magnitudes of the $\Delta G°$ data are quite different in Tables 3 and 6. This disparity also is as expected and as previously observed, since small differences in $\Delta H°$ are magnified when the enthalpy data are used to extrapolate $\Delta G°$ to a common reference temperature (30 °C here) which

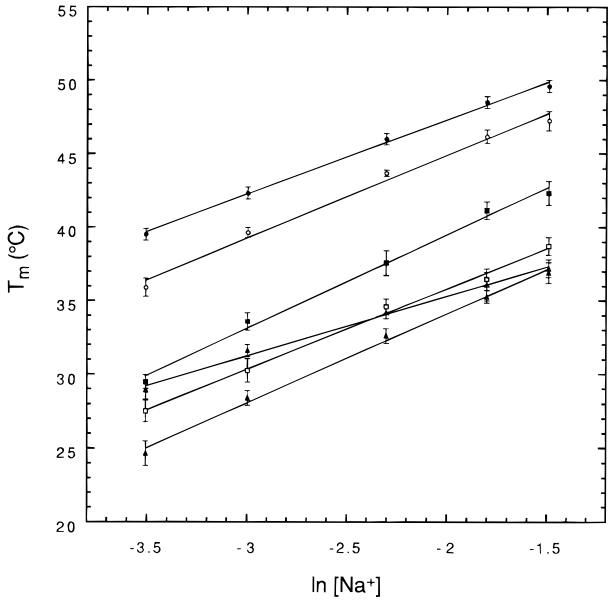

FIGURE 8: Plots of T_m as a function of $[Na^+]$ for all six duplexes. (Filled circles) $A_1{\cdot}T_2$; (open circles) $AP_1{\cdot}T_2$; (filled squares) $AP_1{\cdot}C_2$; (open squares) $AP_1{\cdot}A_2$; (filled triangles) $AP_1{\cdot}G_2$; and (open triangles) $A_1{\cdot}C_2$. Data points and error bars represent the means and standard deviations of three independent determinations. Lines are the results of linear least-squares analyses. Experimental conditions are $C_T = 7\ \mu$M, 10.0 mM PO_4, 1.0 mM EDTA, pH 7.0.

Table 5: Salt Dependence of the Helix-to-Coil Transitions

duplex	dT_m/d ln $[Na^+]$	Δi^a
$A_1{\cdot}T_2$	5.08 ± 0.11	0.108 ± 0.003
$AP_1{\cdot}T_2$	5.64 ± 0.22	0.108 ± 0.008
$AP_1{\cdot}C_2$	6.39 ± 0.25	0.125 ± 0.008
$AP_1{\cdot}A_2$	5.56 ± 0.25	0.099 ± 0.005
$AP_1{\cdot}G_2$	6.04 ± 0.20	0.115 ± 0.006
$A_1{\cdot}C_2$	4.04 ± 0.24	0.077 ± 0.005

[a] Values of Δi were determined using the ΔH_{vH} values in column 3 of Table 3. However, use of the ΔH_{cal} values does not alter the relative Δi order.

is distant from the T_m values. Significantly, however, these extrapolations do not alter the relative $\Delta G°$ values; in other words, the $\Delta G°$ hierarchies remain the same. Consequently, the $\Delta\Delta G°$ values derived from the optical and the calorimetric data should be and are similar, as we observe and discuss below.

DISCUSSION

Comparison of the Relative Thermodynamic Stabilities of Duplex Base Pairs with DNA Polymerase-Mediated Insertion Frequencies. It has been proposed that the rate of insertion by DNA polymerases of an improper base relative to the proper one is determined by differences in stability between the newly formed mismatched site and the corresponding normal Watson−Crick base pair [see Galas and Branscomb (1978) and Goodman et al. (1993) and references cited therein]. As described above, our spectroscopic and calorimetric data on average reveal the difference in stability ($\Delta\Delta G°$) between the $A_1{\cdot}T_2$ and $AP_1{\cdot}T_2$ duplexes to be 0.5 kcal mol^{-1} at 30 °C. This $\Delta\Delta G°$ value can be compared with 1.1 kcal mol^{-1}, the $\Delta\Delta G°$ predicted from the ratio of insertion frequencies of AP versus A opposite T (Clayton et al., 1979). Considering the potential errors inherent in the analysis, we consider this agreement to be quite good. The

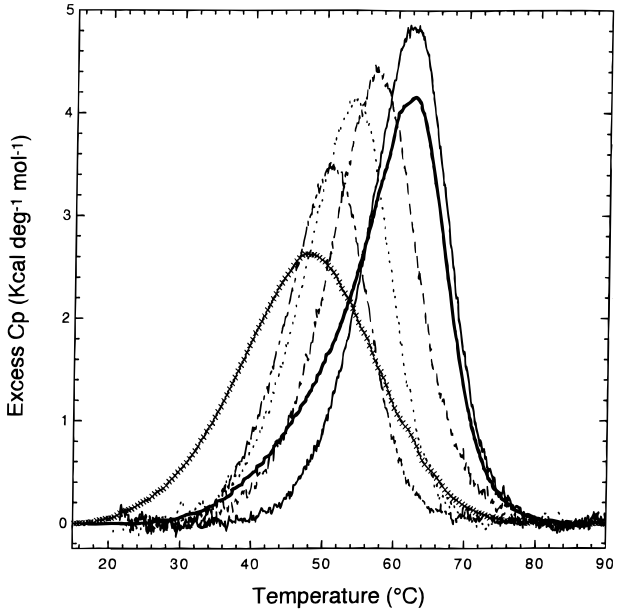

FIGURE 9: Excess molar heat capacity as a function of temperature as determined by DSC. (Thick line) $A_1{\cdot}T_2$; (thin line) $AP_1{\cdot}T_2$; (dashed line) $AP_1{\cdot}C_2$; (dotted line) $AP_1{\cdot}A_2$; (− · −) $AP_1{\cdot}G_2$; (− × −) $A_1{\cdot}C_2$. Experimental conditions are 50.0 mM PO_4, 1.0 mM EDTA, and 1.00 M Na^+, pH 7.0. Values of C_T ranged from 2.3×10^{-4} to 2.5×10^{-4} M.

Table 6: Calorimetrically Derived Thermodynamic Data

duplex	ΔH_{cal} (cal mol$^{-1)}$	ΔS_{cal} (cal K^{-1} mol^{-1})	$\Delta G_{cal30°C}$ (cal mol^{-1})
$A_1{\cdot}T_2$	74050 ± 2700	220 ± 8	7357 ± 3629
$AP_1{\cdot}T_2$	71175 ± 1755	212 ± 5	6907 ± 2318
$AP_1{\cdot}C_2$	70810 ± 4250	215 ± 13	5633 ± 5795
$AP_1{\cdot}A_2$	66165 ± 4535	202 ± 14	4929 ± 6211
$AP_1{\cdot}G_2$	51120 ± 865	158 ± 3	3222 ± 1255
$A_1{\cdot}C_2$	62388 ± 1567	195 ± 5	3274 ± 2180

free energy difference, $\Delta\Delta G°$, between the $AP_1{\cdot}T_2$ and $AP_1{\cdot}C_2$ duplexes determined from both our calorimetric and optical melting curves (∼1.2 and 1.2 ± 1.0 kcal mol^{-1}, respectively) also favorably compares with each other and with the value of ∼1.8 kcal mol^{-1} predicted from the ratio of insertion frequencies of C versus T opposite AP (Watanabe & Goodman, 1982).

In the aggregate, the qualitative consistency between the thermodynamically and kinetically determined free energy differences for AP·T vs A·T and AP·C vs AP·T base pairs lends support to a model in which nucleotide insertion discrimination by DNA polymerases is influenced strongly by equilibrium differences in base pairing stabilities. However, one also must consider the properties of the enzyme, including constraints within the active site of the polymerase, which, as previously noted, may enable discrimination at the nucleotide insertion step at a level which exceeds predictions based solely on free energy differences determined in solution (Petruska & Goodman, 1985; Petruska et al., 1986). Indeed, for the natural base pairs, A·C versus A·T, the $\Delta\Delta G°$ value of ∼3.7 kcal mol^{-1} that we calculate (Table 2) predicts a dAMP·C misinsertion efficiency of about 2×10^{-3}. However, the observed misinsertion efficiencies range from approximately 5×10^{-4} ($\Delta\Delta G° \sim 4.6$ kcal mol^{-1}) for *Drosophila* DNA polymerase α to 5×10^{-5} ($\Delta\Delta G° \sim 5.9$ kcal mol^{-1}) for avian myeloblastosis reverse transcriptase (Mendelman et al., 1989). The magnitudes of these error frequencies were observed to depend both on the identity of the polymerase and on nearest-neighbor primer/template base stacking interactions. Thus, along with differences in thermodynamic stabilites of base pairs and mispairs, the properties of the enzyme also appear to play a significant role in establishing the magnitudes of polymerase misinsertion errors.

Inspection of the optically-derived data in Table 2 and the calorimetrically-derived data in Table 6 reveals the difference in $\Delta G°$ values (at 30 °C) between the $AP_1{\cdot}C_2$ and $AP_1{\cdot}A_2$ duplexes to fall between 0.7 and 1.4 kcal mol^{-1}. This result is consistent with the findings that incorporation of AP opposite A occurs at a significantly lower efficiency than incorporation of AP opposite C (Mhaskar & Goodman, 1984). In a previous study of heptameric duplexes with either AP·C or AP·A as the central base pair (with the rest of the sequence being identical), the AP·A-containing duplex exhibited a higher T_m than the AP·C-containing duplex (Eritja et al., 1986). In our study, the AP base is flanked on both sides by C residues, while in the Eritja et al. (1986) study, the AP base is flanked on both sides by G residues. This difference could account for the observed differential behaviors since nearest-neighbor interactions are known to contribute significantly to the overall stability of a DNA duplex (Breslauer et al., 1986), while also having been shown to play an important role in the rates of nucleotide insertion (Bloom et al., 1993; Mendelman et al., 1989; Petruska & Goodman, 1985) and excision (Bloom et al., 1994; Petruska, & Goodman, 1985) by DNA polymerases. Thus, it is possible that the differences in T_m hierarchy between the work of Eritja et al. (1986) and the present work can be attributable to differences in nearest-neighbor interactions, particularly differences in transition enthalpy. However, both systems involve an unusual base (AP) which is not part of existing thermodynamic databases. Consequently, a quantitative analysis of the nearest-neighbor interactions for these duplexes currently is not possible. This work begins the process of expanding the existing thermodynamic database to include the AP residue.

Presence of an AP·C Site Causes Less Duplex Destabilization than an A·C Site. Inspection of the $\Delta\Delta G°$ data listed in Table 2 reveals that, relative to the parent $A_1{\cdot}T_2$ duplex, the duplex with the central A·C mismatch is destabilized by 3.7 kcal mol^{-1}, while the corresponding duplex with the cental $AP_1{\cdot}C_2$ is destabilized by only 1.9 kcal mol^{-1}. In other words, the mismatch site with the modified base both thermally (ΔT_m) and thermodynamically ($\Delta\Delta G°$) is less destabilizing than the corresponding mismatch without the modified base. This observation may be a general consequence of base modification, since we previously have noted a similar effect for the 8-oxoguanine and propano-dG lesions, when no significant conformational change occurs to accommodate the lesion site (Plum & Breslauer, 1994; Plum et al., 1992, 1995). Perhaps the pairing schemes of the Watson−Crick interactions evolved to maximize the thermodynamic cost of creating a mismatch error, thereby providing an energetic basis for differential recognition and repair (Pilch et al., 1995; Plum & Breslauer, 1994; Plum et al., 1995; Eichols & Goodman, 1991).

Local versus Global Melting. Whereas a UV equilibrium melting curve monitors global duplex dissociation, a fluorescence melting profile monitors local duplex perturbations in the vincinity of the fluorophore, in this case the AP

residue. In Figure 6, we compare the melting behaviors of the four AP-containing duplexes as monitored by UV absorbance (the lines) and fluorescence (the symbols), with the apparent T_m differences being listed in column 3 of Table 4. Note that for both the $AP_1 \cdot C_2$ and $AP_1 \cdot A_2$ duplexes, the differences between the T_m values derived from the UV- and fluorescence-monitored melting curves are negligible. This observation is consistent with local perturbation of the helix around the AP residue and global disruption of the duplex being coincident equilibrium events. By contrast, we observe a difference in both the shape and the T_m values for the UV-monitored and fluorescence-monitored melting curves of the $AP_1 \cdot T_2$ duplex, with the transition as monitored by fluorescence being narrower and occurring entirely within the temperature range of the UV transition. These latter observations may reflect duplex regions outside the domain of the central fluorophore melting over a broader temperature range. Subtle local changes in rigidity and solvent accessibility near the fluorophore prior to global duplex melting also may be influencing the sharpness of the fluorescence signal. However, one should keep in mind that the temperature-dependent fluorescence data may be influenced by transient kinetic states that are not reflected in the equilibrium properties. Independent of any molecular interpretation, it is clear that global melting of the $AP_1 \cdot T_2$ duplex as defined by UV absorption and local melting as defined by AP fluorescence are not coincident equilibrium events. For the $AP_1 \cdot G_2$ duplex, the difference between the T_m values determined from the UV and fluorescence melts is even larger (2.5 ± 0.4 °C), with the fluorescence-monitored transition occurring at a distinctly lower temperature than the UV absorbance-monitored transition. This differential behavior is consistent with the AP fluorophore domain in the $AP_1 \cdot G_2$ duplex being perturbed locally prior to global duplex melting. In this connection, it is interesting to note that for heptameric duplexes containing a central AP·G mismatch, it has been proposed that the AP base is extrahelical (Guest et al., 1991). While our results cannot address this structural issue, both our data and those of Guest et al. (1991) are consistent with an AP·G site forming a locally perturbed domain within a DNA duplex.

Salt-Dependent Melting Studies at Neutral pH Are Consistent with the AP·C Site Being Unprotonated and the A·C Site Being Protonated. For nucleic acid helix-to-coil transitions such as those studied here, Record and co-workers (Record et al., 1978) have defined the parameter Δi, which represents the change in the thermodynamic degree of ion dissociation upon melting, which can, in part, be viewed as reflecting differences in the average axial charge densities between the initial and final states. To assess if the presence of the modified base and the identity of its cross-strand partner might alter Δi, we have measured the salt dependence of the melting transition for the six duplexes listed in Table 1B. Inspection of the resulting data in Table 5 reveals that our measurements and calculations, assuming equivalent final states, reveal little, if any, variation in Δi between the duplexes studied, with the exception of the $A_1 \cdot C_2$ duplex. Note that both the $\partial T_m/\partial \ln [Na^+]$ and Δi values for the $A_1 \cdot C_2$ duplex are significantly lower than those for all the other duplexes, particularly the $AP_1 \cdot C_2$ duplex. One event that could result in such lower values is base protonation at the A·C site in the duplex state, although other mismatch-induced structural alterations in the duplex could provide alternative explanations.

In connection with the foregoing discussion, some time ago it was proposed that the AP·C mismatch is protonated at neutral pH (Sowers et al., 1986a). However, a very recent NMR study using ^{15}N-labeled duplexes has shown, at neutral pH, that the AP·C, in fact, does not exist in a protonated Watson−Crick state, but rather forms a Wobble base pair (Fagan et al., 1996). Since a protonated base pair would reduce the overall charge density of the duplex, the values of $\partial T_m/\partial \ln [Na^+]$ and Δi for a duplex with a protonated base pair should be less than those in an unprotonated state. However, we observe no such reduction, with the $AP_1 \cdot C_2$ duplex actually exhibiting the highest $\partial T_m/\partial \ln [Na^+]$ and Δi values. Thus, our salt-dependent data at neutral pH are consistent with an unprotonated AP·C base pair in the $AP_1 \cdot C_2$ duplex and a protonated A·C base pair in the $A_1 \cdot C_2$ duplex, although alternative explanations clearly are possible. Consistent with the latter conclusion based on our salt-dependent melting data, the NMR results of Goodman and co-workers (Sowers et al., 1986b) have shown that an A·C mismatched site can exist in a protonated Wobble form.

Intensity of the Negative CD Band at 255 nm May Reflect the Stability of AP-Containing Duplexes and/or the Strength of the AP·X Base Pair. Panel B of Figure 7 shows the CD spectra of the $AP_1 \cdot X_2$ family of duplexes. Note that we observe significant quantitative differences in the intensities of the negative band around 255 nm, with the following order of decreasing intensity: $AP_1 \cdot T_2 \approx AP_1 \cdot C_2 > AP_1 \cdot A_2 > AP_1 \cdot G_2$. This order matches that of decreasing overall duplex stability as reflected by the $\Delta G°$ data in the final columns of Tables 3 and 6. As described below, it may be possible to correlate empirically the intensity of the 255 nm CD band measured here with the strength of the interaction between the AP residue and its opposing base as defined by time-resolved fluorescence decay measurements which monitor the internal motion of the AP residue in a family of heptamers, in which AP is opposite T, C, A, or G (Guest et al., 1991).

The results of Guest et al. (1991) show the variation of the correlation time for the internal motion of AP with temperature to be strongest when AP is paired with T or C, weaker when AP is paired with A, and weakest when AP is paired with G. Since the Guest et al. (1991) measurements were made in a temperature range within which the duplex to single-strand transition occurs for each duplex, the authors suggest that the degree of variation of the internal correlation time with temperature reflects the strength of the interaction between the AP residue and its opposing base. From their analysis, they propose the order of decreasing "base pair" strengths to be AP·T ≈ AP·C > AP·A > AP·G. Inspection of panel B of Figure 7 reveals that this order agrees with the order we observe for the CD intensity at 255 nm for the four AP-containing duplexes. In other words, at least for this family of duplexes, the intensity of the CD band at 255 nm may reflect the degree of interaction of the AP residue with its opposing base. We recognize that this correlation may be fortuitious and that additional studies are required to assess the generality, if any, of this observation.

CONCLUSIONS

We have performed a complete thermodynamic analysis of six duplexes, four of which contain the nucleotide analog

2-aminopurine (AP). Our calorimetric and optical data reveal the order of duplex stability to be $A_1{\cdot}T_2 > AP_1{\cdot}T_2 > AP_1{\cdot}C_2 > AP_1{\cdot}A_2 \geq AP_1{\cdot}G_2 \geq A_1{\cdot}C_2$. The values we measure for the free energy differences between the $A_1{\cdot}T_2$ and $AP_1{\cdot}T_2$ duplexes, and between the $AP_1{\cdot}T_2$ and $AP_1{\cdot}C_2$ duplexes, represent a significant fraction of the predicted $\Delta\Delta G°$ values based on *in vitro* data derived from misinsertion frequencies by DNA polymerases. Consequently, our data are consistent with a model in which nucleotide insertion discrimination by DNA polymerases is significantly influenced by the stabilities of the newly formed base pairs, although the actual magnitudes of polymerase misinsertion errors also will depend on enzyme properties.

REFERENCES

Aboul-ela, F., Koh, D., & Tinoco, I., Jr. (1985) *Nucleic Acids Res. 13*, 4811−4824.

Bessman, M. J., Muzyczka, N., Goodman, M. F., & Schnaar, R. L. (1974) *J. Mol. Biol. 88*, 409−421.

Bloom, L. B., Otto, M. R., Beechem, J. M., & Goodman, M. F. (1993) *Biochemistry 32*, 11247−11258.

Bloom, L. B., Otto, M. R., Eritja, R., Reha-Krantz, L. J., Goodman, M. F., & Beechem, J. M. (1994) *Biochemistry 33*, 7576−7586.

Breslauer, K. J. (1995) *Methods Enzymol. 259*, 221−242.

Breslauer, K. J., Frank, R., Blöcker, H., & Marky, L. A. (1986) *Proc. Natl. Acad. Sci. U.S.A. 83*, 3746−3750.

Clayton, L. K., Goodman, M. F., Brascomb, E. W., & Galas, D. J. (1979) *J. Biol. Chem. 254*, 1902−1919.

Connolly, B. A. (1991) in *Oligonucleotides and analogues. A practical approach* (Eckstein, F., Ed.) pp 155−183, IRL Press, Oxford, U.K.

Eichols, H., & Goodman, M. F. (1991) *Annu. Rev. Biochem. 60*, 477−511.

Eritja, R., Kaplan, B. E., Mhaskar, D., Sowers, L. C., Petruska, J., & Goodman, M. F. (1986) *Nucleic Acids Res. 14*, 5869−5884.

Fagan, P. A., Fàbrega, C., Eritja, R., Goodman, M. F., & Wemmer, D. E. (1996) *Biochemistry 35*, 4026−4033.

Fazakerley, G. V., Sowers, L. C., Eritja, R., Kaplan, B. E., & Goodman, M. F. (1987) *Biochemistry 26*, 5641−5646.

Freese, E. (1959) *J. Mol. Biol. 1*, 87−105.

Frey, M. W., Sowers, L. C., Millar, D. P., & Benkovic, S. J. (1995) *Biochemistry 34*, 9185−9192.

Galas, D. J., & Branscomb, E. W. (1978) *J. Mol. Biol. 88*, 653−687.

Goodman, M. F., Creighton, S., Bloom, L. B., & Petruska, J. (1993) *Crit. Rev. Biochem. Mol. Biol. 28*, 83−126.

Gralla, J., & Crothers, D. M. (1973) *J. Mol. Biol. 73*, 497−511.

Guest, C. R., Hochstrasser, R. A., Sowers, L. C., & Millar, D. P. (1991) *Biochemistry 30*, 3271−3279.

Krug, R. R., Hunter, W. G., & Grieger, R. A. (1976) *J. Phys. Chem. 80*, 2335−2341.

Marky, L. A., & Breslauer, K. J. (1987) *Biopolymers 26*, 1601−1620.

Mendelman, L. V., Boosalis, M. S., Petruska, J., & Goodman, M. F. (1989) *J. Biol. Chem. 264*, 14415−14423.

Mhaskar, D. N., & Goodman, M. F. (1984) *J. Biol. Chem. 259*, 11713−11717.

Muzyczka, N., Poland, R. L., & Bessman, M. J. (1972) *J. Biol. Chem. 247*, 7116−7122.

Olmsted, M. C., Anderson, C. F., & Record, M. T., Jr. (1991) *Biopolymers 31*, 1593−1604.

Petruska, J., & Goodman, M. F. (1985) *J. Biol. Chem. 260*, 7533−7539.

Petruska, J., Sowers, L. C., & Goodman, M. F. (1986) *Proc. Natl. Acad. Sci. U.S.A. 83*, 1559−1562.

Pilch, D. S., Plum, G. E., & Breslauer, K. J. (1995) *Curr. Opin. Struct. Biol. 5*, 334−342.

Plum, G. E., & Breslauer, K. J. (1994) in *DNA Damage: Effects of DNA Structure and Protein Recognition* (Wallace, S. S., Houten, B. V., & Kow, Y. W., Eds.) pp 45−56, The New York Academy of Sciences, New York.

Plum, G. E., Grollman, A. P., & Breslauer, K. J. (1992) *Biochemistry 31*, 12096−12102.

Plum, G. E., Grollman, A. P., Johnson, F., & Breslauer, K. J. (1995) *Biochemistry 34*, 16148−16160.

Record, M. J., Jr., Anderson, C. F., & Lohman, T. M. (1978) *Q. Rev. Biophys. 11*, 103−178.

Rogan, E. G., & Bessman, M. J. (1970) *J. Bacteriol. 103*, 622−633.

Snell, F. D., & Snell, C. T. (1949) *Colorimetric Methods of Analysis*, 3rd ed., p 671, Van Nostrand, New York.

Sowers, L. C., Fazakerley, G. V., Eritja, R., Kaplan, B. E., & Goodman, M. F. (1986a) *Proc. Natl. Acad. Sci. U.S.A. 83*, 5434−5438.

Sowers, L. C., Fazakerley, G. V., Kim, H., Dalton, L., & Goodman, M. F. (1986b) *Biochemistry 25*, 3983−3988.

Watanabe, S. M., & Goodman, M. F. (1982) *Proc. Natl. Acad. Sci. U.S.A. 79*, 6429−6433.

BI9614545